Strojniški vestnik - Journal of Mechanical Engineering 60(2014)7-8, 495-505
DOI:10.5545/sv-jme.2013.1393
Original Scientific Paper
Received for review: 2013-08-20
Received revised form: 2013-12-23
Accepted for publication: 2014-01-24

Modeling Thermal Oxidation of Coal Mine Methane in a Non-Catalytic Reverse-Flow Reactor

Xiaoni Qi[1] – Yongqi Liu[1,*] – Hongqin Xu[2] – Zeyan Liu[1] – Ruixiang Liu[1]

[1] Shandong University of Technology, College of Traffic and Vehicle Engineering, China
[2] Shandong University of Technology, College of Mechanical Engineering, China

Inspired by detailed designs of industrial porous burners, the combustion of methane–air mixtures in a non-catalytic reverse-flow reactor was studied numerically. The governing equations are the unsteady state equations of conservation of mass and chemical species, with separate energy equations for the solid and gas phases. These equations were solved using the commercial CFD code Fluent. In order to reveal the actual thermal oxidation in porous media, the user defined function (UDF) is used to extend the ability of FLUENT. The model has been used to investigate the effects of operating conditions such as the mixture inlet approach velocity (0.15 to 0.8 m/s) and methane concentration (0.3 to 0.7%) on the oxidation of methane within non-catalytic reactors packed with ceramic monolith blocks under adiabatic conditions. The calculated values of methane conversion showed good agreement with the corresponding available experimental data. Moreover temperature distribution characteristics in the oxidation bed were studied in order to maintain the autothermicity of TFRR with a high enough temperature in the hot zone.

Keywords: lean-methane, reverse flow reactor,thermal oxidation, modeling

0 INTRODUCTION

Coal mine methane is not only a greenhouse gas but also a wasted energy resource if not utilised. As the air volume is large and the methane resource is dilute and variable in concentration and flow rate, ventilation air methane is the most difficult source of CH_4 to use as an energy source. Because methane concentration in mine ventilation air is usually below 1 vol.% [1], the combustion of lean methane-air mixtures combined with the recovery of the heat of reaction is an important problem for the mining industry. Since the flowrates of this air from a single ventilation shaft usually exceed 500,000 m^3/h, the methane gas should be somehow utilized rather than released into the atmosphere. One of the most reasonable options seems to be the combustion of CH_4 in reverse-flow reactors with simultaneous heat recovery. A number of studies have been carried out to determine the best ways to utilize this lean methane via combustion and to recover the energy thus produced. Due to the very low CH_4 concentrations the most promising solution seems to be autothermal combustion in reverse-flow reactors.

The combustion products of CH_4 are CO_2. Although CO_2 is also a greenhouse gas, its global warming potential is 21 times lower than that of CH_4. So far, most studies have focused on catalytic combustion in catalytic flow-reversal reactors (CFRRs). The first attempt at ventilation air methane (VAM) combustion in CFRR was supposedly carried out at the Boreskov Institute of Catalysis [2]. At present CANMET in Canada is the most advanced in terms of the development of the technology of lean air-methane mixtures combustion [3] and [4]. The principles of catalytic combustion and the general developments in the field have been described in a number of review articles [5] to [7]. Until now, many scholars [8] to [14] have studied the lean methane catalytic oxidation in a reverse flow reactor. Hayes [8] examined the combustion of methane on a palladium catalyst in a monolith reactor and determined the rate equation. Pablo M. [9] systematically compared the performance of particle beds and monolithic beds in catalytic reverse flow reactors. Shi [10] classified the existing technologies for coal mine methane mitigation and utilisation. Hayes [11] developed a comprehensive 2-D finite-element model for a single channel of a honeycomb type monolith catalytic reactor. Aubé [12] developed a mathematical model of CFRR that combines a transient two-dimensional heterogeneous model with a numerical method allowing the fast formulation of new reactor configurations during the design phase. Tischer [13] developed transient two- and three-dimensional simulations of catalytic combustion monoliths. Veser [14] presented a one-dimensional two-phase reactor model for the oxidation of methane to synthesis gas over platinum in a monolith reactor. Shahamiri [15] developed a one-dimensional model to investigate the effects of operational conditions on CFRR. The authors in [16] studied the combustion of preheated lean mixtures of hydrogen with methane in a catalytic packed-bed reactor, it was demonstrated that the one-dimensional model could predict the effects of changes in operating conditions on the methane

*Corr. Author's Address: Shandong University of Technology, College of Traffic and Vehicle Engineering, Zhangzhou Road 12, Zibo 255049, China, bmjw@163.com

and hydrogen conversions, species concentrantions and gas temperature profiles along the bed. The simulations and experimental studies [17] performed show that CFRRs are characterised by high operating temperatures, leading to possible deactivation or even destruction of the relatively expensive catalyst.

Some investigations [18] and [19] carried out a comparative assessment of TFRR and CFRR. It has been shown that both solutions have advantages and drawbacks. Should the heat recovery be seriously taken into account, thermal flow-reversal reactors (TFRRs) are economically and technically the most advantageous solution. Therefore, non-catalytic oxidation in TFRRs is now frequently regarded as an attractive alternative [20]. Such reactors have long been used, e.g. for the homogeneous (thermal) combustion of volatile organic compounds (VOCs) [21]. However, obvious differences exist between the combustion of VOCs and the oxidation of ventilation air methane in reverse-flow reactors. In the former case, no heat is withdrawn from the system. Thermal combustion in a TFRR should be carried out under conditions that do not promote excessive formation of NO_x , i.e. at temperatures below a maximum of 1300 °C in the reactor. The use of a TFRR for the combustion of lean methane mixtures therefore requires detailed studies to determine the reasonable operating conditions. The objective of the present study is to develop a model of reactive flow within a non-catalytic bed packed with ceramic monolith blocks, which include adequate heat and mass transfer models and consider both simultaneous gas phase and surface reactions. Such a model can be applied to investigate the effects of key operational parameters on thermal oxidation processes within the bed reactor, including the effect of fuel composition. It can also be used in combination with experimental data in deriving much needed data for thermal oxidation operations when employed in industry.

1 PHYSICAL AND MATHEMATICAL DESCRIPTION OF THE PROBLEM

A schematic diagram of the honeycomb ceramic bed being considered in the simulation and experiment is shown in Fig. 1. The computational region, of which the length is 2100 mm, the section is 600×600 mm squared, which includes the porous ceramic block with a pore size is 2 to 3 mm. In a reverse flow reactor the feed is periodically switched between the two ends of the reactor using switching valves. When switching valves 1 and 4 are open, the feed flows to the reactor from left to right (forward flow), indicated by the solid arrows. When switching valves 2 and 3 are open, the feed flows to the reactor from right to left (reverse flow), indicated by the dotted arrows. The total cycle consists of these two operations, and the term switch time denotes the time elapsed between two consecutive flow reversals. The sum of the times for forward and reverse flow is the cycle time. Thermal energy generated in an exothermic methane oxidation reaction can be captured with a solid heat storage medium. Then, by switching the flow direction, it is possible to keep the reactor core at high reaction temperatures. Therefore, autothermal operation is possible even when working with cold lean feeds. A one-dimensional physical model is presented here. A premixed homogeneous fuel/air mixture enters a reactor packed with noncatalytic honeycomb ceramic monolith blocks. The bed is initially at a uniform temperature.

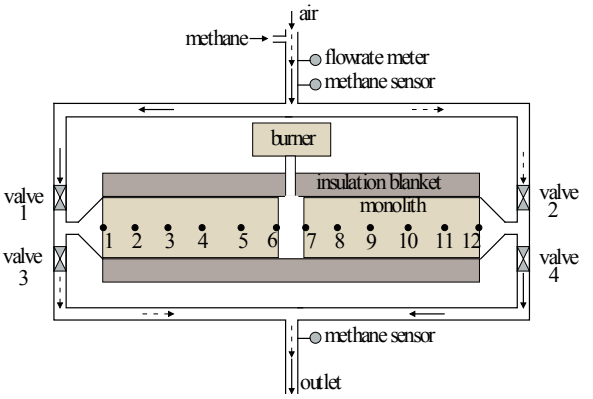

Fig. 1. *TFRR operating principle and experimental schema*

The products formed leave the surface via a desorption process and travel from the surface to the gas mixture via mass diffusion. A portion of the heat released due to surface reactions increases the solid temperature, while the remainder is transferred to the gas phase. The heat received by the gas phase may be high enough to promote gas phase reactions.

The three modes of heat transfer (conduction, convection and radiation) contribute jointly to the transport of heat within the reactor. Conduction redirects heat from the downstream to the upstream regions of the bed, which contributes to an additional preheating of the fuel-air mixture. Convective heat transfer provides heat exchange between the solid and gas phases while the radiation mode becomes important mainly at sufficiently high temperature levels.

The transport processes taking place within the reactor are complex and the following assumptions

are employed in the developed model. The reactor operates adiabatically and at atmospheric pressure. The flow in the reactor is assumed to be one-dimensional. The gas and solid are not in local thermal equilibrium. Therefore, separate energy equations are considered for each phase. Radiation heat transfer in the gas phase is considered to be negligible in comparison to the solid ceramic radiation. The reactants and the products are treated as incompressible ideal gases. The thermophysical properties of the gas species are functions of the local temperature and composition while those of the ceramic are assumed to be uniform and temperature independent. Based on these assumptions the governing conservation equations of mass, energy, and species are as follows:

Conservative equation:

$$\frac{\partial \rho_g}{\partial t} + \frac{\partial (\rho_g u_g)}{\partial x} = 0. \quad (1)$$

Species balance equation:

$$\rho_g \frac{\partial Y_{g,i}}{\partial t} + \rho_g u_g \frac{\partial Y_{g,i}}{\partial x} = -\rho_g D_{i,m} \frac{\partial^2 Y_{g,i}}{\partial x^2} + \\ + \frac{k_{i,m}}{\varepsilon} a_c \rho_g \left(Y_{s,i} - Y_{g,i} \right) + M_i \dot{R}_{g,i}, \quad (i = 1, \cdots, N_g), \quad (2)$$

$$k_{i,m} \rho_g \left(Y_{g,i} - Y_{s,i} \right) = M_i \dot{R}_{g,i}, \quad (i = 1, \cdots, N_g). \quad (3)$$

Heat balance equation for the gas phase:

$$\rho_g c_g \frac{\partial T_g}{\partial t} + \rho_g c_g u_g \frac{\partial T_g}{\partial x} = \\ = -k_g \frac{\partial^2 T_g}{\partial x^2} + \frac{h}{\varepsilon} a_v \left(T_s - T_g \right) + \sum_{j=1}^{N_g} M_j \dot{R}_{g,j} H_j. \quad (4)$$

Heat balance equation for the solid phase:

$$\rho_s c_s \frac{\partial T_s}{\partial t} = -k_s \frac{\partial^2 T_s}{\partial x^2} + \frac{\partial q_{rad}}{\partial x} + \frac{h}{1-\varepsilon} a_v \left(T_g - T_s \right). \quad (5)$$

Ideal gas law:

$$\rho_g = \frac{R T_g}{p M_g}. \quad (6)$$

The diffusion coefficients, $D_{i,m}$ for each species (Eq. (2)) are obtained using Taylor-Aris dispersion theory [22], convective mass transfer coefficient, $k_{i,m}$, (Eqs. (2) and (3)) are calculated by analogy to the Taylor-Aris dispersion. The value of the thermal conductivity, k_s, (Eq. (5)) is obtained from [23]. The diffusion approximation for radiation is used to consider the effect of radiation heat transfer with q_{rad} (in Eq. (5)) calculated from the Rosseland model:

$$q_{rad} = -\frac{16 \sigma T^4}{3 \beta}, \quad (7)$$

where σ is the Stefan-Boltzmann constant, 5.67×10^{-8} W/(m^2·K^4), and β is the extinction coefficient calculated from [24]:

$$\beta = 1.5 \varepsilon_r (1-\varepsilon) \frac{S_r}{d_H}, \quad (8)$$

where ε_r is the emissivity of the honeycomb ceramic, ε is the porosity of the bed and S_r is the scaling factor calculated as:

$$S_r = 1 + 1.84(1-\varepsilon) + 3.15(1-\varepsilon)^2 + 7.2(1-\varepsilon)^3, \quad (9)$$
$$\varepsilon > 0.3.$$

The flow in the monolith channel is laminar and entrance effects may be significant. The Nusselt number for heat transfer is calculated from the correlation of Groppi and Tronconi [25]. For square channels the Nusselt number is given by:

$$Nu = h d_H / k_s = 2.977 \left(1 + 3.6 Gz^{1/2} e^{(-50/Gz)} \right). \quad (10)$$

The Graetz number is:

$$Gz = (d_H \cdot \mathrm{Re} \cdot \mathrm{Pr}) / x. \quad (11)$$

The Reynolds number and Prandtl number are given by:

$$\mathrm{Re} = u d_H \rho_g / \mu_g, \quad (12)$$

$$\mathrm{Pr} = c_{p,g} \mu_g / k_g. \quad (13)$$

The local heat transfer coefficient is calculated from the local Nusselt number using the hydraulic diameter as the characteristic length. At the beginning of each new monolith section a new entry length is assumed to start.

The area to volume ratio for a monolith is calculated using the fractional open frontal area, or porosity, of the monolith structure and the hydraulic diameter of the channels.

$$a = 4 \varepsilon / d_H. \quad (14)$$

The pressure drop is neglected and the velocity is corrected for temperature as follows:

$$u_s = u_{s,inlet} T_g / T_{g,inlet}. \quad (15)$$

The velocity, u_s, is defined in terms of the superficial velocity, which is based on the empty cross sectional area and the interstitial velocity, u, is the actual fluid velocity in the void space, thus:

$$u = u_s / \varepsilon. \tag{16}$$

The fluid is treated as an ideal gas, the density, heat capacity, thermal conductivity and viscosity of the fluid are described by a third-order polynomial function of temperature.

The boundary and initial conditions are:

- Boundary conditions:

$$x = 0 : T_g(x,t) = T_{g,inlet},$$
$$h(T_g(x,t) - T_s(x,t)) = -k_s \frac{\partial T_s(x,t)}{\partial x},$$
$$Y_g(x,t) = Y_{g,inlet} \tag{17}$$

$$x = L : \frac{\partial T_g(x,t)}{\partial x} = 0,\ \frac{\partial T_s(x,t)}{\partial x} = 0,\ \frac{\partial Y_{g,i}(x,t)}{\partial x} = 0. \tag{18}$$

- Initial condition:

$$t = 0 : T_g(x) = T_{g,inlet},\ T_s(x) = T_{g,inlet},\ Y_i(x) = Y_{i,inlet}. \tag{19}$$

In this simulation, the initial temperature of the porous medium is set to the temperature distribution function in the oxidation bed after the startup process finished. The initialization of oxidation bed temperature field was realized by importing the UDF program in Fluent.

2 NUMERICAL METHOD

Because the intermediate reaction products and the generation of free radicals are not involved, the single-step oxidation of the methane reaction mechanism will not affect the accuracy of the reaction heat of the reaction and reaction residence time. The governing equations (Eqs. (1) to (6)) for a ceramic packed-bed reactor could not be solved directly using the commercial software Fluent. However, some features of this code such as the QUICK scheme and second order method for discretization of temporal terms and easier post-processing of the numerical results contain useful code for solving Eqs.(1) to (6). The heat and mass transfer coefficients (e.g. Eqs (10)), which are not predefined in the software, were computed via modifying subroutines (UDFs). The values for these coefficients were updated at every flow time step. At each flow time step, t, the numerical integration of this system was performed while the flow variables were considered to remain unchanged. Therefore, the rate of depletion or generation of the gas phase species i due to the surface reactions over this time interval is:

$$\dot{R}_{s,i} = \frac{X_{g,i_g}^{t+\Delta t} - X_{g,i_g}^{t}}{\Delta t}. \tag{20}$$

This value was then substituted in Eqs. (3) and (4) for the numerical solution. Correspondingly, the amount of heat release due to surface reactions (Eq. (5)) was calculated. The same procedure of integration was performed for the gas phase reactions $\dot{R}_{g,j} = \frac{dX_j}{dt}$.

The steady state solution for each condition was sought using the system of equations that are, nevertheless, in transient form. This was carried out by performing an adequate number of iterations until the solution reached a steady state operating point.

Fig. 2. *Sketch of part of the computational domain and the meshes*

8000 computational cells for spatial discretization of the domain and a time step of 10^{-5} s were used in the simulations.

As the grids were refined, the results did not change significantly, which means that the current density of the grid sensitivity is low, the results meet the need. Fig. 2 shows the grids in the computational domain.

3 EXPERIMENTAL REACTOR SYSTEM

Tests of methane thermal oxidation were carried out in a reverse flow reactor built at the Energy Research Institute of Shandong University of Technology. A general view of the experimental apparatus is shown in Fig. 3, while a simplified flowsheet of the apparatus is given in Fig. 4. The reactor is 600 mm wide, 600 mm high and 2100 mm long. Thermal energy generated in an exothermic methane oxidation reaction can be captured using the solid heat storage medium. Then, by switching the flow direction, it is possible to keep the reactor core at high reaction temperatures.

Therefore, autothermal operation is possible even when working with cold lean feeds.

In the experiments, the ceramic honeycomb monoliths were used as the heat storage medium. The monoliths consist of a structure of parallel channels with porous walls. The properties of monolith are shown in Table 1.

Table 1. *Properties of the honeycomb monolith*

Property	Value
Width of square hole [mm]	2.25
Wall thickness [mm]	0.7
Density [kg/m^3]	2400
Specific surface area [m^2/m^3]	1005
Porosity [Void/%]	57
Thermal conductivity [W/(m·K)]	8
Heat capacity [J/(kg·K)]	1200
Bearing temperature [^{0}C]	1350

Fig. 3. *General view of the research & demonstration TFRR apparatus*

The oxidation bed is packed with ceramic monolith blocks with a large number of straight and parallel channels (2×2 to 3×3 mm), resulting in a low pressure drop. To prevent heat loss from the reactor to the surroundings, the reactor was surrounded with a layer of insulation ceramic fiber blanket 350 mm thick. The thermal conductivity of the ceramic fiber blanket is 0.144 W/(m·K). Therefore, heat loss from the outer surface can be ignored.

As shown in Fig. 4, the complete cycle consists of these two operations to ensure the symmetry of the temperature field of the TFRR.

Thermal profiles from the reactor were obtained using twelve thermocouples (denoted from 1 to 12 in Fig. 4). All thermocouples were placed along the centerline of the reactor. The data acquisition system recorded all sensor values.

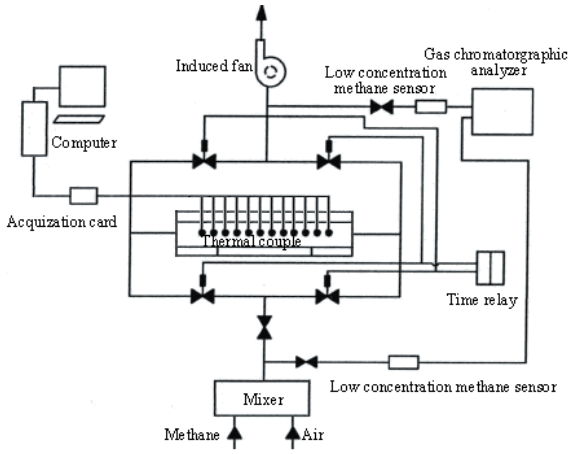

Fig. 4. *General overview of the research & demonstration TFRR apparatus*

The experimental system is divided into four parts: gas supply system, temperature acquisition system, startup system, gas composition analysis system and oxidation bed body. A schematic diagram of the experimental apparatus is shown in Fig. 4. Mine ventilation air used in the experiment was a mixture air and natural gas, where CH_4 purity is 99.9%. Compressed air from the air compressor through the gas regulating valve and pressure-relief valve mixes with the methane from Methane cylinder in the mixer, which is then fed into the oxidation bed. The time relay controls the periodic closing and opening of the electromagnetic valve to control the the cycle gas flow direction. To initiate the reaction, the reverse flow reactor was preheated from an ambient temperature to about 950 °C using an electrical heater in the central position of the reactor. Once the reactor was preheated, the burner was extinguished and the lean methane mixture was supplied to the reactor. The heating temperature and heating power in the startup process is controlled by the temperature control instrument. The intake and exhaust composition is tested by gas chromatography. Electric heaters mounted in the middle of TFRR were used only for preheating the monoliths to enable the start of normal operations. There are 12 thermocouple measuring points arranged along the axis of the oxidation bed, the output signal of the thermocouple connected to the computer can monitor the transient temperature field in the TFRR. The direction of the gas flow was controlled by four solenoid valves.

After the experimental system is well connected, and the experimental instrument, equipment and airtightness is checked, the experiment is started. The experimental procedures are as follows:

(1) Turn on the power switch of the device, the system is then connected to the electricity supply and the air compressor is turned on;
(2) Turn on the time relay, set the commutation switch time, and the reversing control system begins to work. Turn on the computer that is connected with the data acquisition card; open the data acquisition operating system on the computer, set the required acquisition channels and parameters, and the values of each parameter are displayed online;
(3) open the methane cylinder and adjust the pressure-relief valve;
(4) then open both the valves for air and for methane and set to the desirable flow rate values;
(5) the device runs on a fixed commutation time, the system starts up successfully;
(6) adjust the operating parameters, according to the experimental conditions, and collect and record the data. Repeat the above process for the next set of condition;
(7) when the experiment is finished, first turn off the methane gas. Turn off the methane pressure-relief valve, stop data acquisition, and store the experimental data, then shut down the computer;
(8) close the flowmeter and then turn off the air source, close the periodically reversing control system. Turn off the control power supply;
(9) for the next experiment, repeat the above operations.

4 RESULTS AND DISCUSSION

4.1 Model Validation

The experimental data we obtained were used to validate the developed model. Simulations were then conducted for the same operational conditions in the same reactor as those employed in the experimental investigation. Fig. 5 shows the centreline temperature profiles obtained from the experiments and the simulations at three times when the methane concentration is 0.5% volumetric concentration in air with a superficial velocity of 0.5 m/s and the switch time is 150 s. The lines represent the simulations and the points the experimental values. The results are in good agreement with the experimental value obtained for the same reactor. Therefore, this model is sufficient for use in the thermal design of objects on a larger industrial scale.

4.2 Temperature Distribution Characteristics in the Oxidation Bed

Fig. 5 shows the numerical results for a mixed gas flow velocity of 0.5 m/s, methane concentration of 0.5% (by volume), and a switching time of 150 s. The abscissa and the ordinate of Fig. 5 represents the axial position in the oxidation bed and the temperature value, respectively. The curves indicate the regenerator temperature profile along the flow direction at 3, 63 and 123 s. The premixed low concentration methane-air mixture is induced into the preheated ceramic honeycomb bed. After a warming-up period caused by the chemical combustion reaction and the heat and mass transfer between the gas and solid, when the temperature of TFRR gets to about 900 °C, methane begins to react. The bed temperature begins to rise because of the heat generated by the oxidation reaction, which, in turn, maintains the oxidation reaction of methane. The bed temperature is higher in the middle and lower on both sides in the axial direction. After switching direction several times, a transient temperature profile that forms an M-shaped curve moves slowly along the axial direction. The curve is steep in the middle part and the curve's moving velocity is much smaller than the feed velocity. It is the same as the wave propagation in physics, which is shown in Fig. 5. The curve parameters, i.e. peak temperature, the average temperature, the moving speed and the shape of the temperature distribution curve, determine the oxidation performance of the TFRR system, which suggests that the relationship between operating parameters and the curve parameters should be further studied.

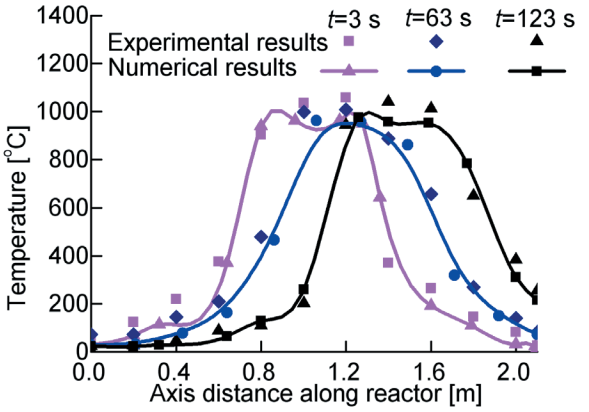

Fig. 5. *Moving curves of the temperature field in the oxidation bed*

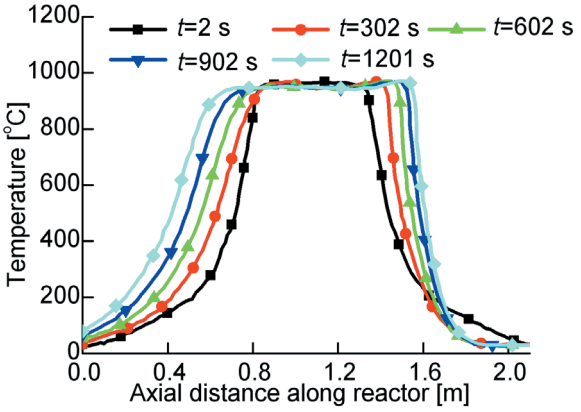

Fig. 6. *Axial temperature distribution as gas flows from left to right at same time in different cycles*

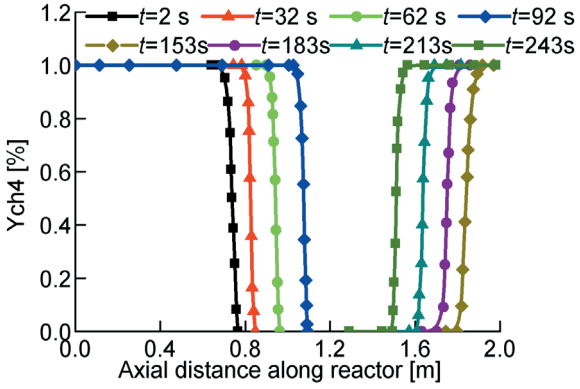

Fig. 7. *Axial CH4 component distribution as the gas flows from left to right and from right to left at different time in the same cycle*

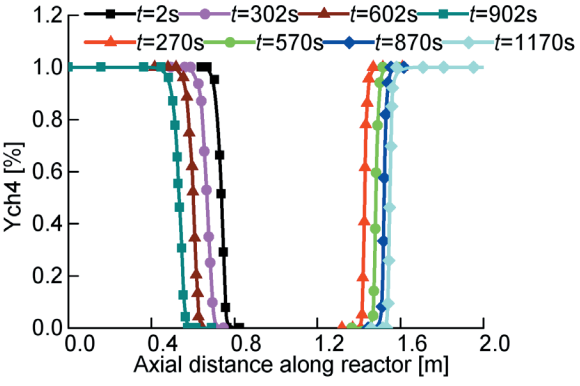

Fig. 8. *Axial CH4 component distribution as the gas flows from left to right and from right to left at the same time in different cycles*

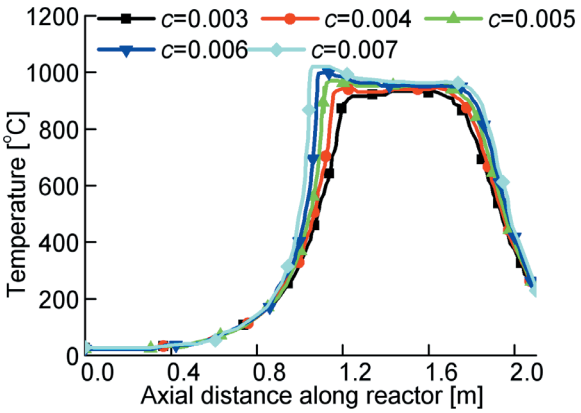

Fig. 9. *Axial temperature distribution as gas flows from right to left within the same cycle*

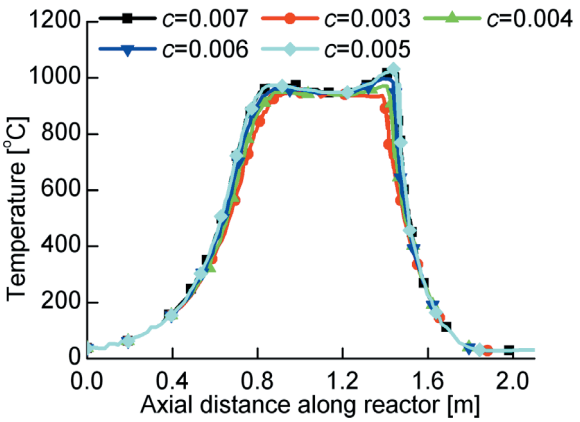

Fig. 10. Axial temperature distribution as gas flows from left to right within the same cycle

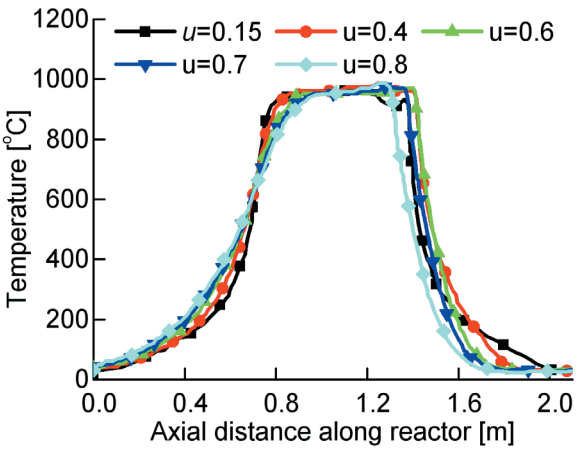

Fig. 11. *Axial temperature distribution as gas flows from right to left at same time in same cycle*

4.3 Changing Principle of Temperature Field and Concentration Fields in the Oxidation Bed over One Cycle

Fig. 6 shows the numerical results for a mixed gas flow velocity of 0.5 m/s, methane concentration of 0.5% (by volume), and a switching time of 150 s. Fig. 6 shows the numerical results for a mixed gas flow velocity of 0.5 m/s, methane concentration

of 0.5% (by volume), and a switching time of 150 s. The curves indicate the gas temperature profile along the flow direction for the first five cycles, i.e. 2, 302, 602, 902 and 1201 s, respectively, when the feed flows from left to right. As can be seen from Fig. 6, with the passage of time the width of the high temperature field obviously increases and the peak value increases slightly. The reason for this is that with the combustion reaction, a large amount of heat is released by burning methane accumulates in the oxidation bed and gradually spreads around so that the scope of the combustion reaction expands and a more involved reaction of methane is prompted, which in turn emits more heat, so that after a few cycles, the temperature distribution will gradually reach the edge of the oxidation bed. If the waveform overflows the oxidation bed, it will cause energy waste.

Fig. 7 shows the numerical CH_4 component distribution results for a mixed gas flow velocity of 0.5 m/s, methane concentration of 0.5%, and a switching time of 150 s. Fig. 7 indicates that the gas temperature profile along the flow direction in the same cycle i.e. 2, 32, 62, 92 and 121 s, respectively, when the feed flows from left to right. In the same cycle, regardless of the gas flow direction, the curve trend is the same. At first, when the bed temperature has not yet reached the temperature of methane combustion, the curve is flat and the methane concentration is 1 (100%) (by volume), ,showing that the methane has not reacted. The more the curve moves to the middle of the bed oxidation, the higher the temperature. The methane then begins to react, so the curve of the methane concentration begins to decrease. Because the methane concentration is very low, the reaction finishes quickly, the methane gas mixture needs to be constantly ireintroduced into the bed, so the curve gradually moves to the middle from one side, then changes direction until the commutation time.

Fig. 8 shows the numerical CH_4 component distribution results for a mixed gas flow velocity of 0.5 m/s, methane concentration of 0.5%, and a switching time of 150 s. There are two sets of curves in the figure, which indicates the methane concentration results of the feed flowing from left to right and from right to left, respectively. Fig. 8 indicates that, while at the same time of different cycles, the curves move to both side, because after one cycle the reaction of methane emits more heat to make the temperature field move to both sides, which promotes a faster reaction of methane and leads the concentration curves to move to the sides. By comparing the two sets of curves, it is shown that the interval of the two sets of curves are different, mainly because over time the gradually increasing resistance leads to a decrease in the mixed gas flow rate, thus the spacing may be reduced.

4.4 Effect of Methane Concentration on Temperature Distribution

Figs. 9 and 10 show the numerical gas temeprature results for a mixed gas flow velocity of 0.5 m/s, methane concentration of 0.3 to 0.7% (by volume), and a switching time of 150 s. Figs. 9 and 10 show that if the other conditions remain the same, when the methane concentration of the mixture varies from 0.3 to 0.7%, i.e. as the concentration increases, the peak temperature is higher, the temperature distribution curve is closer to the inlet side, the high temperature region of the temperature distribution increases, the concavity of the intermediate high temperature region is deeper, and the temperature gradient of the inlet and outlet increases.

The main reason is that when the oxidation bed is working under the high temperature conditions, the higher concentration of methane gas mixture should release a large amount of heat after a quick combustion reaction, but the flow rate does not increase, therfore the heat has little time to transfer to the exit end, so the heat accumulates in the middle to form a prominent peak temperature. However, it is important to note that if the methane concentration is too high, too much heat will accumulate in a local area bringing about a higher temperature which may cause damage to the ceramic regenerator; if the methane concentration is low, very little heat accumulated locally makes the peak temperature decrease, the high temperature zone narrows, the bed temperature began to drop and eventually drops below the critical methane oxidation temperature, resulting in an oxidation reaction that cannot proceed and an oxidation bed that cannot operate properly.

4.5 Effect of Velocity on Temperature Distribution

Fig. 11 shows the numerical gas temeprature results for a mixed gas flow velocity of 0.15 to 0.8 m/s, methane concentration of 0.5% (by volume), and a switching time of 150 s. The effect of feed velocity on the gas temperature distribution is shown in Fig. 11. It indicates that with premixed methane gas flow increasing from 0.15 to 0.8 m/s, the maximum peak temperature and high-temperature zone change little. How can this be?

The effect of the feed velocity on the temperature distribution has two trends. On one hand, when the

concentration of methane is lower, the exothermic heat of the oxidation reaction increases with the flow rate, because for the same oxidation bed, if the methane concentration is fixed, a higher feed velocity means a higher flow rate and the combustion process in the oxidation bed will release more heat, so the temperature of the oxidation bed and the gas rises; on the other hand, the convective heat taken away by the air will increase as the feed velocity is higher. However, this depends on a specific condition: the convective heat being taken away caused by the increasing feed velocity must exceed the increasing thermal effects of oxidation also caused by the increasing feed velocity. Therefore, when operating TFRR, the maximum temperature value cannot be considered to simply change with the increasing or decreasing feed velocity. Therefore, conclusions should be made according to the actual situation in order to guide the actual operation correctly.

6 CONCLUSIONS

The model developed simulates the thermal oxidation of lean homogeneous methane–air mixtures in a reverse flow reactor while employing the user defined function (UDF) to extend the ability of FLUENT. It was demonstrated that the model could predict the effect of changes in operating conditions such as inlet mixture composition, velocity of methane conversions, as well as the species concentrations and gas temperature profiles along the bed. The displayed trends were in good agreement with the corresponding experimentally observed ones.

It is doubtful, if any further complexity of the model, e.g. two-dimensional in space, could easily improve it. The important point is that the agreement of the temperature profiles shown in Fig. 6 seems to be sufficient to ensure good thermal design of objects on a larger industrial scale. The main goal of the design is to maintain autothermicity of TFRR via a high enough temperature in the hot zone, while realising that real CH_4 conversion will be lower due to some other reasons that are hard to include in the model.

The main conclusions of the present study are:

(1) In the TFRR the lean methane mixture ignition takes place at almost 900 °C. The heat release from the combustion of methane increases the gas and solid temperature, which, in turn, maintains the oxidation reaction of methane. The bed temperature is higher in the middle and lower on both sides along the axial direction. After switching direction several times, a transient temperature profile that forms an M-shaped curve moves slowly along the axial direction. The curve is partially steep in the middle part, and the curve's velocity is much lower than the feed velocity. It is as same as the wave propagation in physics.

(2) After several cycles, the width of the high temperature field clearly increases and the peak value increases slightly. With the combustion reaction, a large amount of heat release by burning methane accumulates in the oxidation bed and gradually spreads around so that the scope of the combustion reaction broadens and more and more methane gets involved in the reaction, which, in turn, emits more heat, so that after some time, the temperature distribution will gradually reach the edge of the oxidation bed. If the waveform overflows from the oxidation bed, it will cause energy waste.

(3) Concentration curves move to both sides at the same time in different cycles. The interval of the two sets of curves are different, mainly because over time gradually increasing resistance leads to decreases in the mixed gas flow rate, the spacing may also be reduced.

(4) If the other conditions remain the same, when the methane concentration of the mixture varies from 0.3 to 0.7% (by volume), i.e. as the concentration increases, the peak temperature is higher, the temperature distribution curve is closer to the inlet side, the high temperature region of the temperature distribution increases, the concavity of the intermediate high temperature region is deeper, and the temperature gradient of the inlet and outlet is increased. However, it is important to note that if the methane concentration is too high, too much heat will accumulate in a local area leading to a high temperature that may cause damage to the ceramic regenerator; if the methane concentration is lower, very little heat accumulated locally makes the peak temperature decrease, the high temperature zone then narrows, the bed temperature begins to drop and eventually drops below the critical methane oxidation temperature, thus resulting in an oxidation reaction that cannot proceed and an oxidation bed that cannot operate properly.

(5) The effect of the feed velocity on the temperature distribution has two opposite trends. Therefore, when operating TFRR, the maximum temperature value cannot be considered to simply change with increasing or decreasing feed velocity. Conclusions should be made according to the actual situation in order to guide the actual operation correctly.

6 NOMENCLATURE

a monolith surface area to volume ratio [m²/m³]
c constant pressure specific heat [J/(kg·K)]
d_H hydraulic diameter [m]
$d_{i,m}$ diffusivity of species i [m²/s]
h convective heat transfer coefficient [W/(m²·K)]
H_i enthalpy of species i [J]
k thermal conductivity [W/(m·K)]
$k_{i,m}$ convective mass transfer coefficient of species i [m/s]
M_i molar mass of species i [mol]
p pressure [Pa]
q_{rad} radiative heat flux [W/m²]
R_g species production rate in gas phase [mol/(m³·s)]
R_s species production rate on surface [mol/(m³·s)]
t time [s]
T temperature [K]
u axial velocity [m/s]
x Axial coordinate [m]
Y_i mass fraction of species i [%]

Greek symbols:
β extinction coefficient
ε porosity
ε_r emissivity of honeycomb ceramic
μ viscosity [Pa·s]
ρ density [kg/m³]

Subscript:
g gas phase
s solid
i component i
inlet at the reactor inlet

7 ACKNOWLEDGMENTS

This work was supported by the China National 863 High Technology Fund project (2009AA063202).

8 REFERENCES

[1] Underground Coal Mine Ventilation Air Methane Exhaust Characterization (2010). *U.S. EPA Coalbed Methane Outreach Program*, U.S. EPA, Boston, p. 1-16.

[2] Gogin, L.L., Matros, L.L. Ivanov, A.G. (1990). *Catalytic Combustion in Catalytic Flow-Reversal Reactors*. Nauka, Novosibirsk. (in Russian)

[3] Salomons, S., Hayes, R.E., Poirier, M., Sapoundjiev, H. (2003). Flow reversal reactor for the catalytic combustion of lean methane mixtures. *Catalysis Today*, vol. 83, no. 1-4, p. 59-69, DOI:10.1016/S0920-5861(03)00216-5.

[4] Litto,R., Hayes, R.E., Sapoundjiev, H., Fuxman, A., Forbes, F., Liu,B., Bertrand, F. (2006). Optimization of a flow reversal reactor for the catalytic combustion of lean methane mixtures. *Catalysis Today*, vol. 117, no. 4, p. 536-542, DOI:10.1016/j.cattod.2006.06.013.

[5] Heck, R.M., Farrauto, R.J. (2001). Automobile exhaust catalysts. *Applied Catalysis A: General*, vol. 221, no. 1-2, p. 443-457, DOI:10.1016/S0926-860X(01)00818-3.

[6] Groppi, G., Tronconi, E., Forzatti, P. (1999). Mathematical models of catalytic applications. Catalysis Review: *Science and Engineering*, vol. 41, no. 2, p. 227-254, DOI:10.1080/01614949909353780.

[7] Forzatti, P. (2000). Environmental catalysis for stationary applications. *Catalysis Today*, vol. 62, no. 1, p. 51-65, DOI:10.1016/S0920-5861(00)00408-9.

[8] Hayes, R.E., Kolaczkowski, S.T., Paul, K.C.L., Awdry, S. (2001). The palladium catalyzed oxidation of methane: reaction kinetics and the effect of diffusion barriers. *Chemical Engineering Science*, vol. 56, no. 16, p. 4815-4835, DOI:10.1016/S0009-2509(01)00131-2.

[9] Pablo, M., Miguel, A.G.H., Salvador, O. (2005). Combustion of methane lean mixtures in reverse flow reactors: Comparison between packed and structured catalyst beds. *Catalysis Today*, vol. 105, no. 3-4, p. 701-708, DOI:10.1016/j.cattod.2005.06.003.

[10] Shi, S., Andrew, B., Hua, G., Cliff, M. (2005). An assessment of mine methane mitigation and utilization technologies. *Progress in Energy and Combustion Science*, vol. 31, no. 2, p. 123-170, DOI:10.1016/j.pecs.2004.11.001.

[11] Hayes, R.E., Kolaczkowski, S.T., Thomas, W.J. (1992). Finite-element model for a catalytic monolith reactor. *Computers and Chemical Engineering*, vol. 16, no. 7, p. 645-657, DOI:10.1016/0098-1354(92)80014-Z.

[12] Aubé, F., Sapoundjiev, H. (2000). Mathematical model and numerical simulations of catalytic flow reversal reactors for industrial applications. *Computers and Chemical Engineering*, vol. 24, no. 12, p. 2623-2632, DOI:10.1016/S0098-1354(00)00618-9.

[13] Tischer, S., Correa, C., Deutschmann, O. (2001). Transient three-dimensional simulations of a catalytic combustion monolith using detailed models for heterogeneous reactions and transport phenomena. *Catalysis Today*, vol. 69, no. 1-4, p. 57-62, DOI:10.1016/S0920-5861(01)00355-8.

[14] Veser, G., Frauhammer, J. (2000). Modelling steady state and ignition during catalytic methane oxidation in a monolith reactor. *Chemical Engineering Science*, vol. 55, no. 12, p. 2271-2286, DOI:10.1016/S0009-2509(99)00474-1.

[15] Shahamiri, S.A., Wierzba, I. (2009). Modeling catalytic oxidation of lean mixtures of methane–air in a packed-bed reactor. *Chemical Engineering Journal*, vol. 149, no. 1-3, p. 102-109, DOI:10.1016/j.cej.2008.09.046.

[16] Shahamiri, S.A., Wierzba, I. (2009). Simulation of catalytic oxidation of lean hydrogen-methane mixtures.

International Journal of Hydrogen Energy, vol. 34, no. 14, p. 5785-5794, DOI:10.1016/j.ijhydene.2009.04.077.

[17] *Recovery of Methane from Vent Gases of Coal Mines and Its Efficient Utilization as a High Temperature Heat Source* (2003). European Union Project, Gliwice, p. 100-126.

[18] Gosiewski, K., Matros, Y.S., Warmuzinski, K., Jaschik, M., Tanczyk, M. (2008). Homogeneous vs. catalytic combustion of lean methane-air mixtures in reverse-flow reactors. *Chemical Engineering Science*, vol. 63, no. 20, p. 5010-5019, DOI:10.1016/j.ces.2007.09.013.

[19] Gosiewski, K., Pawlaczyk, A. (2013). Catalytic or thermal reversed flow combustion of coal mine ventilation air methane: What is better choice and when. *Chemical Engineering Journal*, vol. 238, p. 1-254, DOI:10.1016/j.cej.2013.07.039.

[20] Gosiewski, K., Pawlaczyk, A., Jaschik, M. (2012). Thermal combustion of lean methane-air mixtures: Flow reversal research and demonstration reactor model and its validation. *Chemical Engineering Journal*, vol. 207-208, p. 76-84, DOI:10.1016/j.cej.2012.07.044.

[21] Salvadora, S., Commandréa, J.-M., Karab, Y. (2006). Thermal recuperative incineration of VOCs: CFD modelling and experimental validation. *Applied Thermal Engineering*, vol. 26, no. 17-18, p. 2355-2366, DOI:10.1016/j.applthermaleng.2006.02.018.

[22] Taylor, G. (1953). Dispersion of soluble matter in solvent flowing slowly through a tube. *Proceedings of the Royal Society*, vol. 219, no. 1137, p. 186-203, DOI:10.1098/rspa.1953.0139.

[23] Wierzba, I., Depiak, A. (2003). The catalytic oxidation of heated lean homogeneously premixed gaseous-fuel air streams. *Chemical Engineering Journal*, vol. 91, no. 2-3, p. 287-294, DOI:10.1016/S1385-8947(02)00165-1.

[24] Singh, B.P., Kaviany, M. (1992). Modelling radiative heat transfer in packed beds. *International Journal of Heat and Mass Transfer*, vol. 35, no. 6, p. 1395-1397, DOI:10.1016/0017-9310(92)90031-M.

[25] Groppi, G., Tronconi, E. (2000). Design of novel monolith catalyst supports for gas/solid reactions with heat exchange. *Chemical Engineering Science*, vol. 55, no. 12, p. 2161-2171, DOI:10.1016/S0009-2509(99)00440-6.